Electrochimica Acta 527 (2025) 146243

Contents lists available at ScienceDirect

Electrochimica Acta

journal homepage: www.journals.elsevier.com/electrochimica-acta

Experimental and theoretical investigation of L-cysteine influence over the electrodeposition mechanism for a novel sustainable acid copper electroplating formulation

Fabio Biffoli [a,b,*], Pierantonio Corsi [a], Mariano Riccardi [a], Carla Bazzicalupi [a], Marco Bonechi [a,c], Claudio Fontanesi [c,d], Walter Giurlani [a,c], Marco Pagliai [a,c,*], Massimo Innocenti [a,c,e]

[a] Department of Chemistry, "Ugo Schiff", University of Firenze, Via Della Lastruccia 3, Sesto Fiorentino, FI, 50019, Italy
[b] Materia Firenze Lab s.r.l., Gruppo Materia Firenze, Via Delle Fonti 8/E, Scandicci, FI, 50018, Italy
[c] National Interuniversity Consortium of Materials Science and Technology (INSTM), Via G. Giusti 9, Firenze, FI, 50121, Italy
[d] Department of Engineering "Enzo Ferrari", (DIEF), University of Modena and Reggio Emilia, Via Vivarelli 10, Modena, MO, 41125, Italy
[e] Center for Colloid and Surface Science (CSGI), Via Della Lastruccia 3, Sesto Fiorentino, FI, 50019, Italy

ARTICLE INFO

Keywords:
Electroplating
Copper electrodeposition
Cysteine
Molecular dynamics
Density functional theory

ABSTRACT

Despite being widespread all over the manufacturing world, industrial acid copper electroplating exploits the same classes of additives since the second half of the 20th century. This work aims to overtake the classical set of accelerators, suppressors, levelers and inorganic salts (e.g. sodium chloride) with low-cost and sustainable additives that can solve multiple roles. A multidisciplinary approach based on spectroscopy, diffractometry, electrochemistry and computational chemistry is employed to characterize the effects of L-Cysteine and its action mechanism during the electrodeposition. We demonstrate how and why this amino acid can promote both grain refinement and roughness reduction without any other additive or inorganic salt. This result is achieved by considering and analyzing the findings of multiple experimental techniques and comparing them with computational calculations and simulations. Such an approach can open new pathways for designing industrial electroplating procedures, ensuring sustainability.

1. Introduction

The electrodeposition of copper by acid electrolytes represents one of the main industrial electroplating processes, along with nickel plating. Both electronic [1–4] and decorative [5–8] manufacturing companies rely on acid copper (AC) formulations to obtain levelled and compact Cu deposits with good mechanical properties. Also, this is accompanied by the high shininess of the synthesized material which is much appreciated in areas where the aesthetical value is an integral part of the material's performance [9]. The capability of obtaining coatings with such characteristics is due to the addition to the virgin make-up solution (VMS) of organic and inorganic molecules, often called additives, that actively interact with the electrodeposition process. The subdivision of organic additives is represented by the classical trifecta of brightener, leveler and suppressor [10]. Brighteners consist of small molecules, containing at least one sulfur atom, who are responsible for the grain refinement [11,12]; they are also called accelerators due to their ability to enhance the deposition rate by promoting both the deposition rate and the suppressor desorption [13]. Levelers give the capability of reducing the substrate roughness [14] by adsorbing on high current density zones like cusps [15]. Aromatic nitrogen atoms are indicated as the functional group that promotes leveling performances, a low-energy bandgap and a LUMO localized on the nitrogen atom is found to be fundamental as it makes possible the electron acceptor role of the leveler [16,17]. Suppressors, instead, are polyethers (e.g., PPG and PEG) which adsorb on the cathodic surface, rising the onset potential [18]. The suppressor role seems to be to promote the deposition of small ordered grains by slowing down the growth (adsorbing on the cathodic surface and complexing the copper) and to interact synergistically with the brightener [19]. Its mechanism of action is not clear yet, but recent studies on polyethers suppressors revealed the key-role of inorganic salts like NaCl in explain the behavior of the suppressor during the

* Corresponding authors at: Department of Chemistry, "Ugo Schiff", University of Firenze, Via Della Lastruccia 3, Sesto Fiorentino, FI, 50019, Italy.
E-mail addresses: fabio.biffoli@unifi.it (F. Biffoli), marco.pagliai@unifi.it (M. Pagliai).

https://doi.org/10.1016/j.electacta.2025.146243
Received 7 February 2025; Received in revised form 26 March 2025; Accepted 14 April 2025
Available online 15 April 2025
0013-4686/© 2025 The Authors. Published by Elsevier Ltd. This is an open access article under the CC BY license (http://creativecommons.org/licenses/by/4.0/).

electrodeposition, focusing on how those polymers, in conjunction with inorganic ions, could migrate towards the cathodic surface [20] and how they interact with brighteners and metallic ions forming complexes and supramolecular structures [19,21]. Other than Cl^-, another promising inorganic anion studied in literature is Br^- [22,23] but it will be not considered in this work as it is a wastewater contaminant and then not suitable for sustainable industrial applications [24–26]. The most important industrial application of AC electroplating is in the layer interconnection of printed circuit boards (PCBs) by plated through hole process (PTH) [27,28]. Despite the usage of sulfur-containing organic molecules to obtain bright and durable deposits is known since the first half of the 1900 [29–31], the research of new additives and formulations to improve the whole process is still trending today. Understanding the mechanism of action of additives during the electrodeposition process is fundamental to predict novel high-performance sustainable formulations. The interaction of additives with the surface is often threated by a phenomenological approach based on a macroscopic view [32], that is useful to easily understand and rationalize obtained coating-morphology, but it lacks on not bringing quantomechanic into the discussion, leaving out interactions on the atomic and supramolecular scale. One of the more emblematic cases is the role of NaCl, where in the classical mechanism the Cl^- is the main active species of this inorganic additive, overlooking the importance of Na^+. Only recently it was observed how Na^+ is fundamental to the migration of the suppressor to the cathode by forming supramolecular abducts that resemble Na crown-ether complexes [19,20]. On the other hand, theoretical works [33–35] produced on this topic provide fundamental insights on the atomic scale, but they usually focus on single or isolated additives, without considering the complexity of the system and macroscopic effects on industrial conditions. To catch the connections between the atomic/nanoscale and the macroscopic world, it is important to take a multidisciplinary approach that connects diffractometry, different spectroscopic probes and electrochemical analyses where the proposed theories need to be confirmed and rationalized by computational methods and simulation [36,37]. In a previously published paper [21], we presented a protocol that involves X-ray diffractometry (XRD) and photoelectron spectroscopy (XPS), scanning electron microscopy (SEM), cyclic voltammetry stripping (CVS), density functional theory calculations (DFT) and molecular dynamics (MD) simulations to understand the roles of additives of a prototypical AC formulation. From the basis of those results, we selected L-cysteine (L-Cys, structural formula reported in Scheme 1) as a main candidate to a new generation of AC formulations, due the presence of an -SH group that allows for a brightener role, an $-NH_2$ group (protonated at AC working conditions) which should solve the cathode migration problem and diminishing the need of Na^+ ions and the carboxylic branch acting as the suppressor by complexing the copper ions and slowing down the reaction. The advantages of employing one single additive instead of for are multiple, especially on the scale of industry, where variables are less controllable in comparison to a laboratory. Using a single additive means Significantly streamline the quality control of the production process as the only variable is the L-Cys concentration, instead of four concentrations (accelerator, suppressor, leveler and NaCl) and their relative ratio. More explicitly among the benefits we can list an easier analytical process by eliminating matrix effects between additives, a more direct resolution of problems directly

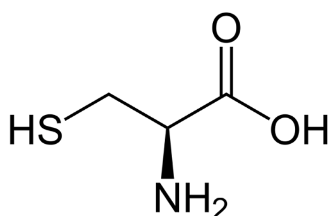

Scheme 1. Structural formula of L-cysteine.

from qualitative analyses such as the Hull cell (just one parameter to adjust), a simplification of wastewater treatment and the reduction of contaminants among the electroplating production line (e.g. Cl^- ions are a key parameter in many electrodeposition processes [38,39]). In addition, NaCl removal greatly simplifies the troubleshooting of problems caused by excess additives, as only activated carbon filtration is needed to restore the bath. L-Cys was already proposed as a promising brightener and suppressor [40], but that formulation was not near to industrial conditions (high copper concentration, low pH and high current densities). Furthermore, L-Cys was also studied as a leveler in a classic AC additive system (brightener, leveler, suppressor and NaCl) [41]. This work aims to propose a one-additive system capable of obtaining uniform, compact and shiny deposits also reducing the substrate roughness and rationalize the mechanisms lying under the synthesis of such material. Atomic force microscopy (AFM) and angle resolved X-ray photoelectron spectroscopy (AR-XPS) were introduced as analytical techniques to study the effects of additives on morphology, surface roughness and to study the configuration of molecules adsorbed on the surface.

2. Materials and methods

2.1. Experimental procedures

The standard electroplating formulation (VMS) was made by a solution of 65 g L^{-1} (0.66 M) of sulfuric acid (96% Merck), and 210 g L^{-1} (0.84 M) copper sulphate pentahydrate (Merck). L-Cys (Merck) was added at different concentrations (0.25 mM, 0.50 mM, 0.75 mM, 1.00 mM, 1.50 mM, 2.50 mM, 5.00 mM) to the VMS.

The galvanostatic mode (current density of 1.75 A dm^{-2}) was selected for the electrodeposition of samples to better simulate the industrial practice. All the samples were electroplated for 10 min. The cathode material was composed by α-β brass plates (exposed surface area 0.19 dm^2) from Ossian Lagerqvist AB (Jarfalla, Sweden) and the anode by phosphorous copper from A.M.P.E.R.E Italia srl (Settimo Torinese, Italy). Phosphorous copper was choose instead of oxygen-free copper as it is the anode material employed in electroplating companies for AC electrodeposition due its corrosion resistant properties that limit the anode solubility, avoiding the copper concentration to rise in the bath. The deposition system involved a parallel arrangement between anode and cathode and air agitation. Prior to electrodeposition the substrate was degreased thanks to an industrial cathodic degreasing solution, ATMETPLUS from Valmet Plating srl (Calenzano, Italy) and rinsed in a pickling solution made of diluted sulfuric acid (5% w/w).

To prove the viability of the proposed formulation on industrial applications a test panel of VMS and one with 5 mM of L-Cys were electroplated in a Hull cell, setting the current density to 1.75 A dm^{-2}. As substrate we employed α-β brass test panels from Ossian Lagerqvist AB (Jarfalla, Sweden) and for Hull cell we used an air agitation tank B-54W from Yamamoto-MS, Co., Ltd (Tokyo, Japan).

The morphology characterization of the electrodeposited films was done by scanning electron microscopy (SEM); Secondary Electron (SE) images were collected with a Hitachi (Tokyo, Japan) SU3800 SEM at 10 kV of acceleration voltage. Then, SE images were processed with ImageJ [42] to obtain the grain dimensions with the linear intercept method [43].

The morphology was also evaluated AFM using a Molecular Imaging PicoSPM (10 μm × 10 μm, 512 px × 512 px, 0.5 lines/s speed) equipped with a non-conductive Veeco NP-S10 silicon nitride triangle-shaped cantilever (spring constant of 0.12 nN m^{-1}). The measurements were done in contact mode with a force setpoint of 0.5 V.

The influence of L-Cys on the crystalline properties of the deposit was investigated by XRD with a Brucker (Billerica, MA, USA) New D8 Da Vinci Diffractometer employing a Cu K_α radiation ($\lambda = 1.54056$ Å), operating at 40 kV and 40 mA. The X-ray diffractometer had a ϑ-2ϑ geometry equipped with a Eulerian cradle and a Brucker LYNXEYEXE

detector. Acquisitions were made in the range 2θ = 40°-100°, using the step size of 0.03° and 0.4 s as integration time a step. The PDF-4+ 2021 database of the International Centre for Diffraction Data (ICDD) [44] was implemented for phases identification on XRD data. The samples were placed parallel to the Eulerian cradle, perpendicular to the normal of incidence, in order to match an eventual preferential direction of growth with the preferential orientation of the crystallites. Hence, the preferential growth orientation was quantified thanks to the relative texture coefficients (RTC) [45,46]. The peak intensities of bulk Cu powder (spacegroup Fm-3m and lattice parameter=3.61 Å) included in the RTC calculation were evaluated thanks to VESTA [47]. RTCs were calculated following Eq. (S2) reported in the Supporting Information.

AR-XPS was used to evaluate the superficial composition of the samples and the configuration of L-Cys adsorbed on top of the surface. The instrument is equipped with a non-monochromatic X-ray source (VSW Scientific Instrument Limited model TA10, Al Kα radiation, 1486.6 eV) set to work at 120 W (12 kV and 10 mA) and a hemispherical analyzer (VSW Scientific Instrument Limited model HA100, Manchester, UK). The analyzer was equipped with a 16-channel detector and a dedicated differential pumping system maintaining the pressure in the chamber to the 10-8 mbar range. The pass energy was set to 44 eV. The measured spectra were analyzed using CasaXPS software. The inelastic background was subtracted using Shirley's method [48] and mixed Gaussian and Lorentzian contributions were used for each component. Calibration of the spectra was obtained by shifting to 284.8 eV, the lowest component relative to the 1s transition of carbon for adventitious carbon [49]. Normalization of the areas subtended by the peaks was carried out using the ASFs (atomic sensitivity factors) by Wagner [50]. Spectra on sample electroplated with L-Cys were taken with the surface tilted at two different angle respect to the normal of incidence: 90° (normal incidence) and 30° (grazing incidence).

A Metrohm (Herisau, Switzerland) μAutolab PGSTAT204 potentiostat/galvanostat, coupled to NOVA 2.1.4 software was employed for Cyclic Voltammetry Stripping experiments (CVS). A three-electrode setup concerning a gold rod counter electrode (CE) an Ag/AgCl saturated KCl (model HI-5312 by Hanna Instruments Woonsocket, RI, USA) reference electrode (RE) and a platinum rotating disk electrode (3 mm of diameter) as a working electrode (WE). The CVSs were performed from +1.5 to −0.25 V, and again back to +1.5 V (versus the reference electrode), with 100 mV/s scan rate, and 2000 rpm rotation speed of the WE, following typical CVS parameters employed for study copper electroplating additives [51,52]. Starting the CVS at a positive potential is needed to desorb any organic molecule on the WE and to ensure the cleaning of it. Then, shifting to more negative potentials (-0.25 V) the copper is electroplated onto the WE. Finally, by coming back to +1.5 V the electrodeposited copper is stripped from the WE, giving an anodic stripping peak from which the charge density is calculated. The charge density, being directly proportional to the electrodeposited mass, as stated by the Faraday's law, is exploited to discuss how additives affect the copper deposition rate. For each experiment three potential cycles have been performed, leading to no significant changes between cycles, thus only the last cycle has been reported in this work. Control experiments on the solution containing 5 mM of L-Cys were done. Specifically one under static conditions (no RDE rotation), one after degassing the cell for 30 min under nitrogen and one without copper sulfate, the results are reported in Fig. S3.

2.2. Computational details

All DFT calculations concerning isolated molecules were performed within the Gaussian 16 framework [53] employing, if not specified otherwise, the Becke three parameter hybrid functional (B3LYP) [54] in conjunction with the D3(BJ) empirical dispersion [55] and the 6-31++G (d,p) split-valence basis set [56–58]. The electronic structure of the molecules was evaluated after a geometry optimization and for the N-protonated L-Cys the chosen conformer was in according to the study of Nacsa and Czako [59].

To verify if the structure hypothesized by AR-XPS could be stable (i.e., a local minimum), a frequency calculation (within the harmonic approximation) after a geometry optimization, performed keeping fixed a Cu (220) surface, was done employing the long-range corrected hybrid functional by Handy (CAM-B3LYP) [60] coupled with the D3(BJ) empirical dispersion. According to literature [61,62], mixed basis-set was selected, concerning the LANL2DZ [63] for Cu atoms and 6-31++G(d,p) for the others.

The tendency of atoms of L-Cys, 1H-Benzotriazole (BTA), thiourea (TU) and Mercaptopropylsulfonic acid (MPS) on donating or drawing electrons was evaluated with the condensed Fukui's indices (calculated following eq(S2) reported in the Supporting Information), employing CM5 charges and 6-31++G(d,p) basis set. The functional influence on Fukui's indices was evaluated benchmarking the N-protonated L-Cys system with the PBE0(D3BJ) [64] local hybrid functional, CAM-B3LYP (D3BJ) and ωB97XD [65] long-range corrected functionals and with the B2PLYP(D3BJ) [66] double hybrid functional.

MD simulations were performed with GROMACS [67] in a 10 nm x 15 nm x 10 nm box with periodic boundary conditions, with a Cu surface oriented towards the (220) phase placed at the bottom of the 10 nm x 10 nm side, filled with 49686 water molecules (TIP3P water model [68, 69]), 100 Cu^{2+} ions, 50 N-protonated L-Cys and 125 sulphate ions. The solid phase was formed by 7 layers of copper for a total of 7840 atoms. The molecular structure of N-protonated L-Cys as already mentioned before and all the topology and force field parameters files [70,71] were generated by the PrimaDORAC web interface [72]. After an energy minimization step, a first equilibration on the NVT ensemble (setting T=300.0 K) was performed incorporating a Nosé-Hoover thermostat [73]. Then, after a previous equilibration step in the NPT ensemble (setting the pressure at 1 atm with a Parrinello-Rahaman barostat [74]), a production run of a total of 10 ns, with a time step of 2 fs was done. During every step an electric field of -0.32 V nm^{-1} was applied in the direction perpendicular to the cathode in order to simulate electrodeposition conditions [21,75].

3. Results and discussion

3.1. Morphological analysis

3.1.1. Scanning electron microscopy

The morphology of electroplated samples obtained with different L-Cys concentration in the formulation (0 mM, 0.25 mM, 0.50 mM, 0.75 mM, 1.00 mM, 1.50 mM, 2.50 mM, 5.00 mM) has been analyzed by secondary electron (SE) imaging. The results reported in Fig. 1 display clearly that L-Cys acts as a grain refiner, reducing both the mean grain size and the size distribution. The grain refinement action follows an exponential dependence as shown in Fig. 1A. This effect is accompanied by a drastic change in the crystal habitus, changing from a hexagonal shape predicted by the Bravais-Friedel-Donnay-Harker (BFDH) and other models that do not consider explicitly the growth environment [76]. By the first addition of L-Cys, it is observable how the grains become smaller, and their morphology changes drastically, resembling an elongated prism, notifying a strong interaction between the organic molecule and the surface. Subsequent additions of L-Cys reduce furthermore the grain dimensions while maintaining the same prism-like habitus. This confirms L-Cys as an effective brightener capable of effectively grain refining the deposit.

3.1.2. Atomic force microscopy

AFM analyses were conducted on the same samples observed at SEM (VMS, 0.25 mM, 0.50 mM, 0.75 mM, 1.00 mM, 1.50 mM, 2.50 mM, 5.00 mM) and on the brass substrate. The results of those experiments are summarized in Fig. 2. The same morphology pattern observed in the previous chapter is also noticeable by the AFM imaging, with elongated grains appearing at the first addition of L-Cys. Additional information

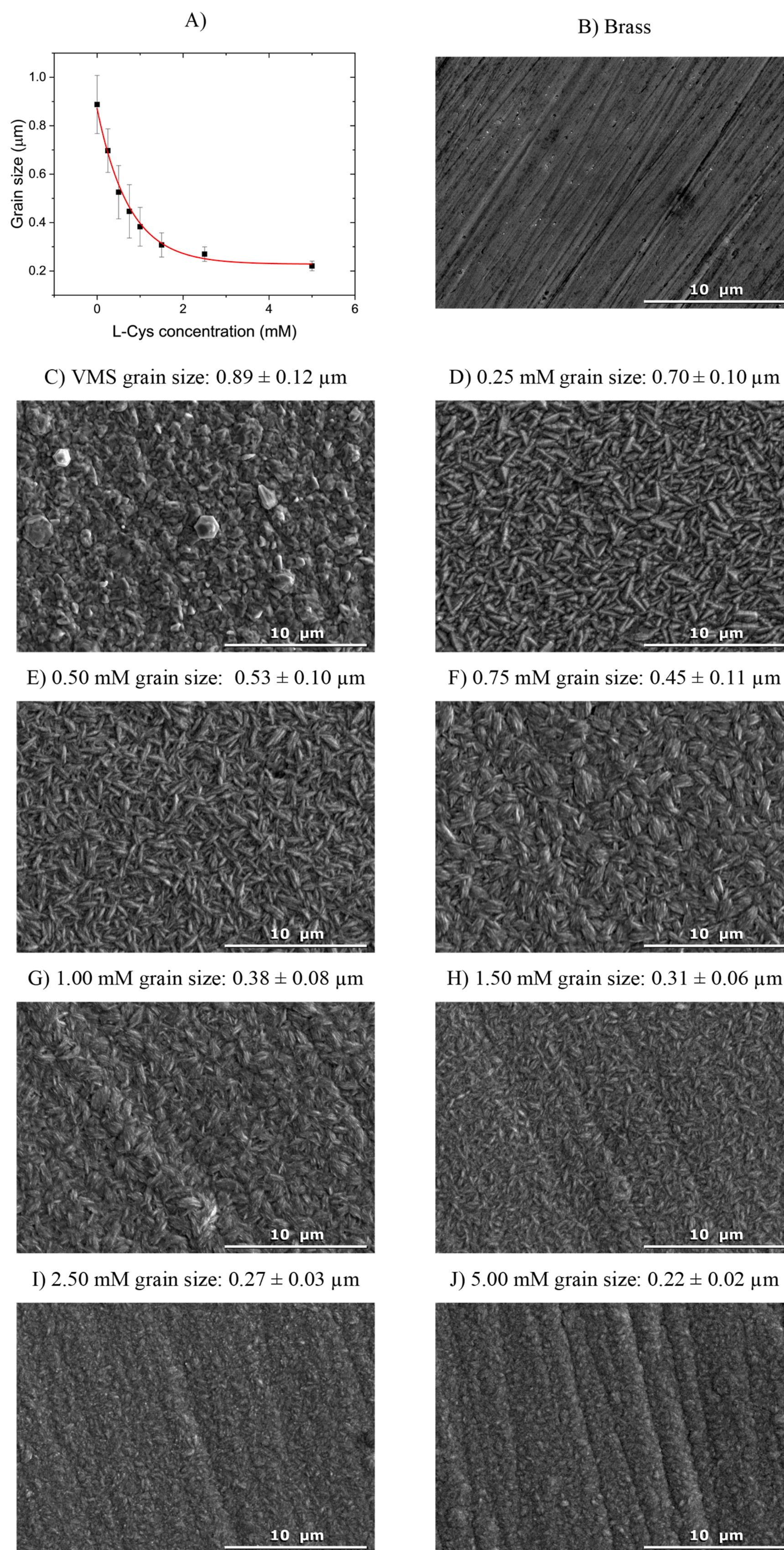

Fig. 1. (A) Correlation between the grain size and L-Cys concentration; (B) non functionalized brass substrate; SEM-SE images obtained on samples electroplated by varying the L-Cys concentration and keeping all other components fixed (VMS formulation: 65 g L^{-1} of sulfuric acid, and 210 g L^{-1} copper sulphate pentahydrate) (C) VMS, (D) 0.25 mM, (E) 0.50 mM, (F) 0.75 mM, (G) 1.00 mM, (H) 1.50 mM, 1.75 (I) 2.50 mM, (J) 5.00 mM. All the electrodepositions were carried out in galvanostatic mode (1.75 A dm^{-2}), under air agitation, for ten minutes as specified in the materials and methods section.

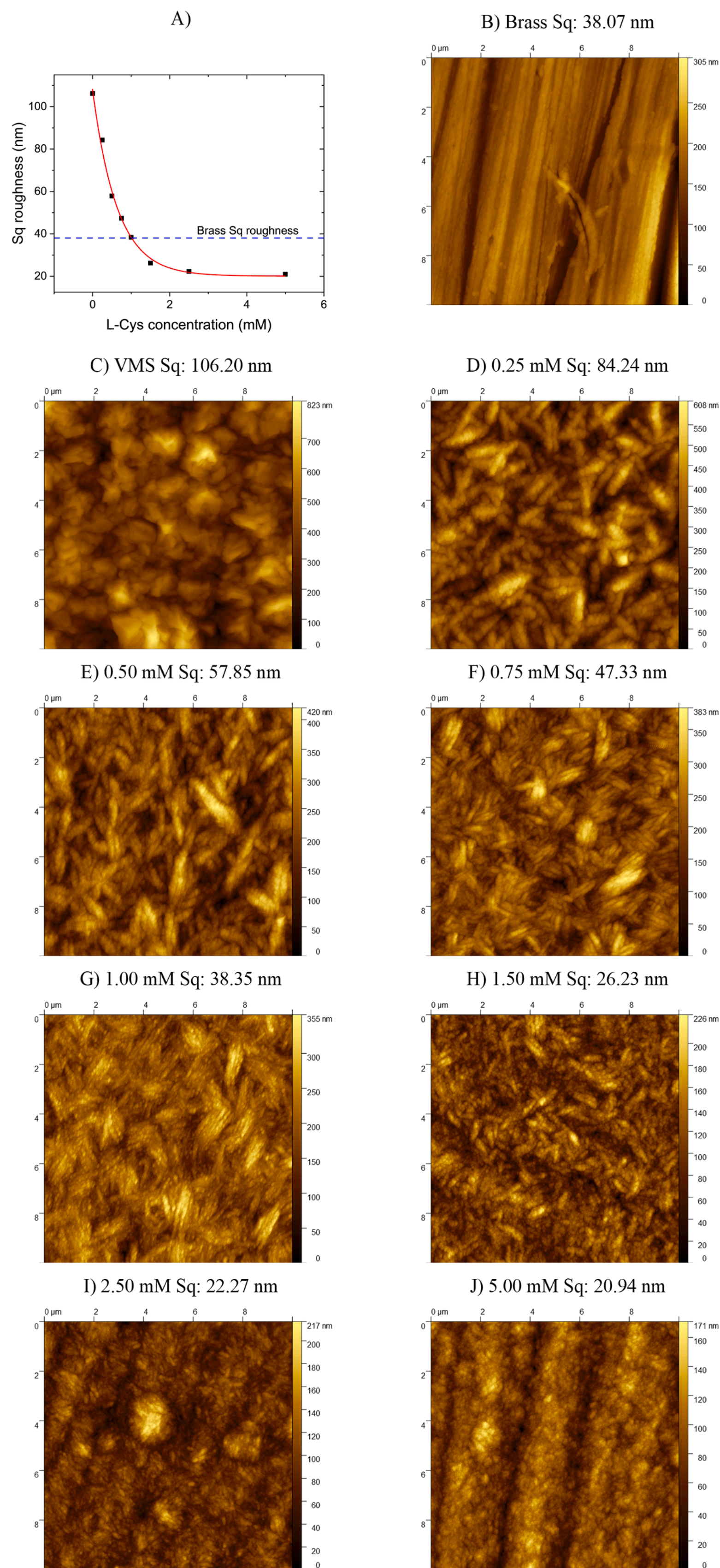

Fig. 2. (A) Correlation between roughness and L-Cys concentration; AFM images obtained (B) on the brass substrate and samples electroplated by varying the L-Cys concentration (C) VMS, (D) 0.25 mM, (E) 0.50 mM, (F) 0.75 mM, (G) 1.00 mM, (H) 1.50 mM, (I) 2.50 mM, (J) 5.00 mM.

can be found observing Fig. 2E-G where the grains tend to align to each other in a preferential direction (i.e., coupling along the lateral side of the prism) forming aggregates. The effect on the roughness of the deposit is displayed in Fig. 2A: the trend of root mean square height (Sq) follows an exponential law like the grain size. Moreover, higher concentration of L-Cys (starting from 1.5 mM) resulted in a levelling effect, lowering the roughness of the brass substrate and underlining how the growth inside the brass “valleys”, that are made by mechanical polishing, is faster than in comparison to the cusps.

3.2. Influence of L-Cys over crystallinity

XRD experiments were performed on the same electrodeposited samples analyzed with SEM and AFM to investigate the influence of L-Cys over crystallinity. From the obtained diffractograms, reported in Fig. S1, it is appreciable how peak positions remain unaltered compared to the calculated Cu powder diffraction pattern. Instead, a major difference is present regarding the relative intensities of the peaks show a deviation from the bulk powder Cu intensity pattern, indicating the presence of preferential orientations. This was quantified by the means of the relative texture coefficient (RTC) and the results are reported in Table 1. A preferential orientation perpendicular to the (220) phase is observed for all samples, VMS included. This is in line with previously reported studies [21,77] as a 2D structure with exposed (220) phase is found to be thermodynamically more stable than others [78].

The first addition of L-Cys enhances the (220) RTC as we would expect from the results of our previous work [21]. Further additions of L-Cys brought a decrease in this estimator, with a minimum of 48.39% for 1.00 mM, and then rises drastically up to 88.08% for the 5.00 mM sample. Linking the XRD results with microscopy, it is possible to speculate how this behavior is related to the presence of aggregates as the rise of (220) RTC corresponds to the disappearance of them (1.50 mM sample).

3.3. Surface composition

The surface composition was characterized thanks to XPS, performing measurements at normal incidence (90°) on a sample obtained from the VMS and one obtained with 5.00 mM of L-Cys. Investigated regions were Cu 2p, N 1s, S 2p, and Cu LMM Auger emission; the chemical state and other spectral features of Cu were processed following the work of Biesinger [79]. For other elements, the Handbook of X-ray Photoelectron Spectroscopy [80] was followed. Fitting parameters and quantification results are reported in Section S2.1 of Supporting Information while the results of the quantitative analysis are in Section S2.2 and Section S2.3 (AR-XPS results). High resolution spectra of Cu 2p region and Cu LMM Auger emission are displayed in Fig. S2 and their angle resolved counterparts in Fig. S3. From the high-resolution spectra of N 1s (Fig. 3A) it is confirmed that the L-Cys adsorbs on the cathodic surface as the nitrogen signal is only present in the L-Cys sample. Furthermore, the effect of the brightener is also observable in Fig. 3B where the addition of L-Cys resulted in an inversion of the S^{2-}/SO_4^{2-} ratio as it shifts from 0.36 (VMS) to 3.16 (L-Cys), hinting again the occurred adsorption. It is also important to underline that the S^{2-} component refers both to organic and inorganic sulfur at that oxidation state (i.e. the sulfur present in L-Cys and the inorganic sulphides).

In Table 2 are summarized the relative concentrations of chemical species on the copper surface. The addition of L-Cys caused the rise of S^{2-} and Cu^{+} this was associated both with the formation of a chemical bond between the sulfur atom of L-Cys and the formation of Cu_2S (investigated with Cu LMM Auger emission) as a product of the L-Cys degradation; the sulfides formation will be discussed more in depth in Section 3.5. The presence of a low concentration of S^{2-} in the VMS sample is due the sulphate reduction that can occurs on top of the Cu surface [21,81].

Angle resolved (AR-XPS) spectra were collected both at normal incidence (90°) and at grazing incidence (30°) on the L-Cys sample. The high-resolution spectra of N 1s and S 2p are reported in Fig. 4 and the relative concentrations of all investigated regions are in Table 3. As no noticeable differences were found, especially considering the measurement uncertainty (Table 3), L-Cys probably adsorbs in a planar configuration, with both sulfur and nitrogen atoms lying on the surface. This opens the possibility of not only the chemical bonding between the S atom and the Cu but also some weak interaction between the surface and N or O which will be discussed in the next section.

3.4. Theoretical results

3.4.1. First principle calculations

The possibility of a stable planar protonated L-Cys adsorbed on the copper surface was confirmed by a geometry optimization and subsequent vibrational frequency calculation which resulted in no imaginary frequencies found, stating the existence of an energetic minimum composed by the molecule planarly adsorbed on a Cu (220) surface; both the geometry and the vibrational frequencies are reported in Section S3.1 of Supporting Information. A comparison between L-Cys and typical additives was done based on analysis of frontier orbitals and atomic Fukui indices [82]; f_a^+ represents the electrophilicity and f_a^- the nucleophilicity of the atom a. Mercaptopropylsulfonic acid (MPS) and thiourea (TU) were selected as standard and well known brighteners while 1H-benzotriazole (BTA) as leveler. To validate the correctness of employing the B3LYP as exchange and correlation functional a benchmark runt over other classes was done due the liability of population analyses over the level of theory [83]. This test confirmed the trend of the Becke three parameters functional (see Section S3.2.1 of Supporting Information). All the data concerning the calculation of Fukui condensed indices, including geometries used and CM5 charges are reported in Section S3.2. In Fig. 5 is reported the frontier orbitals diagram of the considered additives. As stated in the introduction, the bandgap is a good indicator of the adsorption capability of the organic molecule on the metallic surface: smaller the bandgap, higher is the affinity to the surface. The L-Cys bandgap is larger than the one of MPS and TU, two typical brighteners. This is reflected in a higher concentration needed compared to them to obtain a similar grain refinement effect, as typical concentrations for TU and MPS are unlikely to exceed 1 ppm. This fact could be linked to the effectiveness of L-Cys of working without the suppressor, that from our previous study, have also the role of regulating the TU adsorption kinetic. The levelling power of L-Cys, observed by AFM, is confirmed by an LUMO energy comparable to the BTA: a lower LUMO is an important parameter to rationalize the electron acceptor capability that is correlated with the adsorption on higher current density zones, which limits the growth of Cu on cusps.

The condensed Fukui indices are reported in Table 4, from the

Table 1
Influence of the L-Cys concentration on preferential orientation estimated with the RTC.

Cu Phases	RTC (%) at varying the L-Cys concentration							
	VMS	0.25 mM	0.50 mM	0.75 mM	1.00 mM	1.50 mM	2.50 mM	5.00 mM
111	7.23	10.98	9.41	11.20	10.37	10.52	3.23	1.28
200	13.20	1.60	5.97	4.59	11.59	3.64	0.72	0.06
220	56.94	67.64	65.47	60.81	48.39	73.90	83.67	88.08
311	22.62	19.78	19.14	23.40	29.65	11.93	12.38	10.57

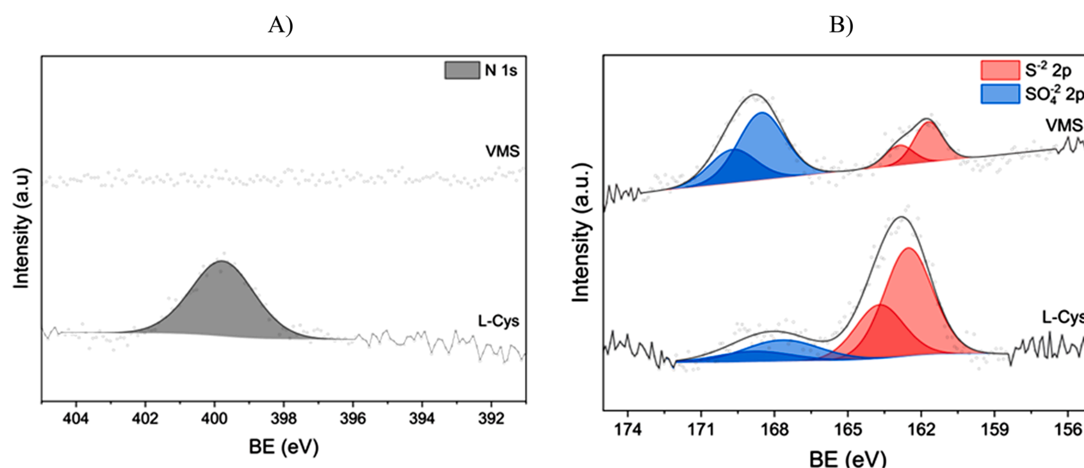

Fig. 3. High resolution XPS spectra of the copper deposit obtained with VMS and L-Cys at normal incidence (90°): (A) nitrogen 1s and (B) sulfur 2p.

Table 2
Relative concentrations of chemical species evaluated from the fitting of high resolution XPS spectra.

Sample	Cu0	Cu^+	Cu tot	N	S^{2-}	SO_4^{2-}	S tot
VMS	54.6 ± 0.5%	40.9 ± 0.4%	95.5 ± 0.9%	-	1.2 ± 0.1%	3.3 ± 0.2%	4.5 ± 0.3%
L-Cys	42.2 ± 0.6%	37.7 ± 0.5%	79.9 ± 1.1%	7.2 ± 0.5%	9.8 ± 0.5%	3.1 ± 0.2%	14.2 ± 0.7%

comparison between the various additives it is clear how brighteners have a strong nucleophilic region corresponding to sulfur atoms; the atoms' numeration employed is referred to the geometries reported in Section S3.2. This, connected to the localized HOMO in that region is reflected in the capability of accelerators in giving chemisorption with the Cu surface as it is already reported in literature. About nucleophilicity, it seems that the levelling power of BTA is correlated to that of nitrogen atoms in which the LUMO is mostly localized. Observing the L-Cys results, both from the frontier orbitals diagram and the condensed Fukui indices, the levelling power of this molecule could be associated not to the nitrogen atom but with the carboxylic group as the LUMO is localized on it and the oxygens have a higher f_a^- compared to the nitrogen. The L-Cys adsorption on Cu and Cu-group metals concerning both the carboxylic group and the sulfur atom was also reported in literature [62,84,85], confirming our findings.

3.4.2. Molecular dynamics calculations

MD simulations were conducted under an electric field perpendicular to the Cu surface to simulate the conditions of the electrodeposition process. The main phenomena investigated were the interaction between L-Cys, Cu^{2+} and sulphate ions in the bulk solution and the physisorption of species on the cathodic surface. This task was accomplished by exploiting both radial and axial distribution functions, the results are reported in Fig. 6.

From Fig. 6A it is observable how L-Cys forms with the sulphate ions a strong first coordination sphere, being both charged. Moreover, L-Cys seems to have three other external coordination spheres, were copper and sulphate ions alternating with each other. This peculiar organization can answer how L-Cys is working without any suppressor as the L-Cys uptake by the surface is regulated by the interactions described before with the sulphate ions, reducing the needs of a kinetic regulator.

Table 3
Relative concentrations of chemical species evaluated from the fitting of AR-XPS spectra.

Angle	Cu^0	Cu^+	Cu tot	N	S^{2-}	SO_4^{2-}	S tot
0°	42.2 ± 0.6%	37.7 ± 0.5%	79.9 ± 1.1%	7.2 ± 0.5%	9.8 ± 0.5%	3.1 ± 0.2%	12.9 ± 0.7%
30°	44.2 ± 0.5%	35.2 ± 0.5%	79.4 ± 1.1%	6.3 ± 0.5%	10.7 ± 0.5%	3.5 ± 0.2%	14.2 ± 0.7%

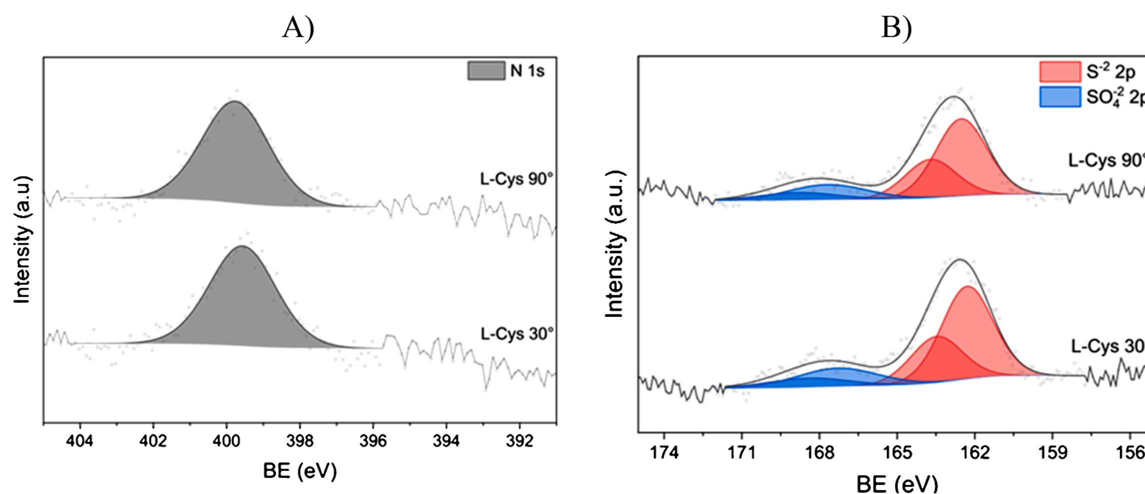

Fig. 4. High resolution AR-XPS spectra of the copper deposit obtained at normal incidence (90°) and grazing incidence (30°) on the L-Cys sample: (A) nitrogen 1s and (B) sulfur 2p.

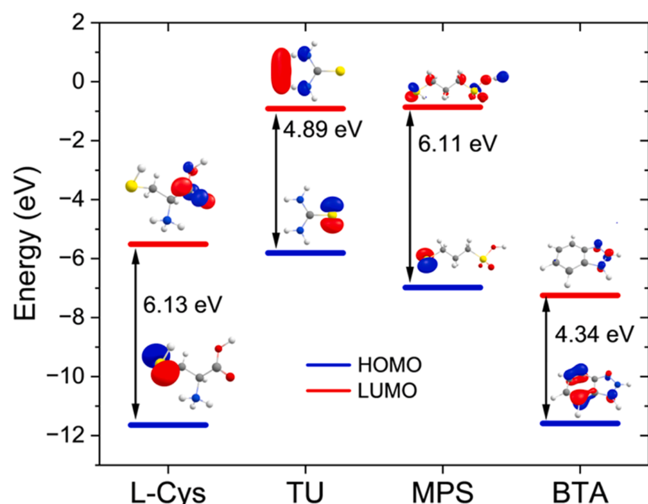

Fig. 5. Frontier orbitals diagram of different copper additives (L-Cys, TU, MPS and BTA); BTA and L-Cys were considered in their protonated form and all the electronic structures were evaluated at B3LYP(D3BJ)/6-31++G(d,p) level.

Table 4
Condensed Fukui indices evaluated thanks to the CM5 population analysis calculated at B3LYP(D3BJ)/6-31++G(d,p) level.

TU	2S	3N	-	-
$f_a^+(q)$	0.629	0.062	-	-
$f_a^-(q)$	0.116	0.050	-	-
BTA	11N	12N	14N	-
$f_a^+(q)$	0.069	0.055	0.079	-
$f_a^-(q)$	0.087	0.111	0.153	-
L-Cys	13S	3N	8O	9O
$f_a^+(q)$	0.492	0.025	0.081	0.027
$f_a^-(q)$	0.089	0.055	0.087	0.051
MPS	1S	13S	-	-
$f_a^+(q)$	0.493	0.029	-	-
$f_a^-(q)$	0.107	0.042	-	-

The suppressor role of Cu complexing agent is also carried by the supramolecular abducts generated by a positively charged molecule like L-Cys in VMS. Giving a look to Fig. 6B the competition between L-Cys and sulphate ions at the cathode (which resembles the competition between a classic brightener and the suppressor) is underlined: the addition of L-Cys causes the desorption of the sulphate ion, as it is replaced by the brightener. In addition, Fig. 6B confirms the physisorption of L-Cys on the copper surface.

3.5. Electrochemical investigation

The electrochemical behavior of the formulation under different L-Cys concentrations was investigated by CVS and the results are reported in Fig. 7. In Fig. S3 control experiments are reported showing how L-Cys do not contribute to the stripping peak current and how both degassing the cell with nitrogen or performing the experiments without WE rotation only affects the electrodeposited copper quantity by reducing it (smaller stripping peaks in comparison to standard CVS). In Fig. 7 it can be observed as the first two addition of L-Cys (0.25 mM and 0.50 mM) enhance the stripping charge density, promoting the copper deposition rate. This "accelerating" behavior in the classical view of copper electrodeposition mechanism is attributed to the competition between the brightener (or accelerator) and the suppressor. In this case, where no suppressor has been used, the rationalization of the phenomenon is given by MD simulations as the suppressor role is taken by the sulphate

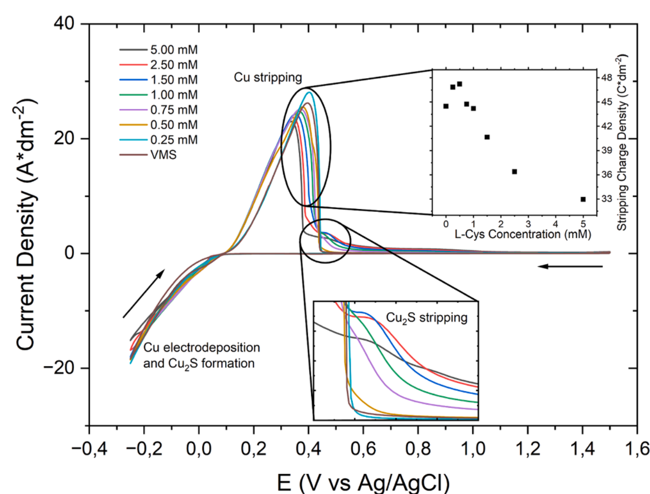

Fig. 7. CVS obtained for the VMS (without additives) and after the addition of different concentration of L-Cys (0.25, 0.50, 0.75, 1.00, 1.50, 2.50, 5.00 mM); a platinum rotating disk electrode (3 mm of diameter) was employed as a WE. The CVSs were performed from +1.5 to −0.25 V, and again back to +1.5 V (versus the reference electrode), with 100 mV/s scan rate, and 2000 rpm rotation speed of the WE. The tested electrolytes are the same employed for galvanostatic depositions and are reported in the materials and methods section.

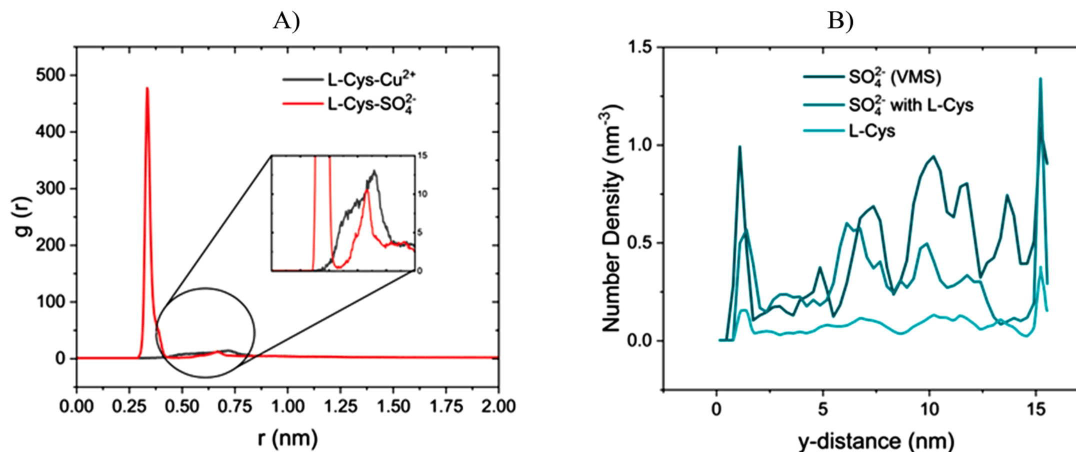

Fig. 6. (A) Radial distribution functions (g(r)) of L-Cys with Cu and sulphate ions; (B) axial distribution function of L-Cys and sulphate ions with and without L-Cys (VMS); to evaluate the distances, the center of mass of the species was considered.

ions and the rising of the anodic peak current can be attributed to the formation of L-Cys first coordination sphere and the diminishing presence of sulphate ions on the cathodic surface that are replaced by the L-Cys, as also observed by XPS with the decreasing of SO_4^{2-} in favor of S^{2-}. Further additions of the additive cause an inversion of the trend, decreasing the stripping charge density and diminishing the copper deposition rate that is proportional to the L-Cys concentration.

At higher L-Cys concentrations (starting from 1.5 mM) a shoulder is observable after the copper stripping peak. This can be ascribed to the stripping of Cu_2S, which presence was confirmed by Auger emission characterization reported in Section S2. The co-crystallization of copper sulfides, especially in grain borders, was already reported in literature [40] and the peak position at higher potential compared to the copper stripping peak is related to a major thermodynamic stability of copper sulfides respect to metallic copper [86,87]. Hence, starting from 1.50 mM of L-Cys added in the formulation, the presence of sulfides in grain border seems to play a key role as it can explain the loss of aggregation formation observed with AFM and the discontinuity in RTC observed in the XRD, due the loss of the second preferential growth direction (see Section 3.1.2).

3.6. Hull cell plating test

To prove the versatility and macroscopic aspect of the proposed formulation a Hull cell panel test was performed both with the VMS and with the formulation containing 5 mM of L-Cys (the one with smaller grains and lower roughness); the results are shown in Fig. 8.

It can be appreciated how the L-Cys addition was capable of giving a homogeneous shiny and reflective deposit all along the Hull panel. This ensures the possible implementation of this bath in industrial facilities as it is capable of giving good deposits in a wide range of current densities, a characteristic that is fundamental in factories, such as the decorative industry, where substrate geometries are mostly irregular and complexes, with many cusps and valleys representing zones with different local current densities. This property is also helpful in the electronic industry as the electric field changes drastically within holes.

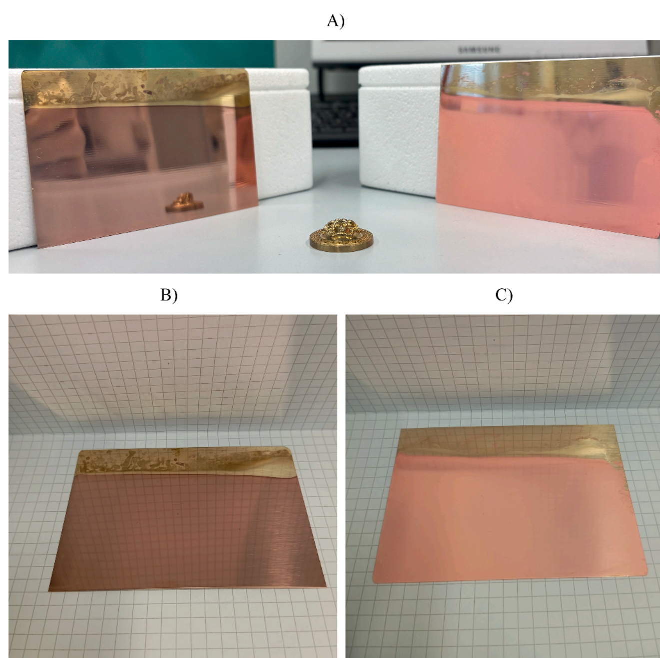

Fig. 8. (A) Comparison of Hull cell panels electroplated with L-Cys 5 mM (left) and VMS (right) with an average current density of 1.75 A dm-2; details of singular Hull cell panel (B) L-Cys 5 mM and (C) VMS.

4. Conclusion

A novel electroplating formulation for acid copper electroplating was proposed and investigated. L-Cys was selected to replace the classic suppressor-accelerator-sodium chloride trifecta due to its peculiar structure and properties. We obtained an electrodeposition solution capable of plating polycrystalline copper with compact and small grains on brass, also reducing the substrate roughness which can be helpful both for electronic and decorative industry, especially considering the total amount of organic content and variables in electroplating baths. Limiting the number of additives is not only helpful in simplifying the treatment of wastewater, but it also makes maintenance and quality control easier for the operator, going to lessen the amount of non-conforming production workpieces. The morphology was analyzed both by SEM and AFM, underlying how the L-Cys works as a grain refiner. Both the grain dimension and the surface roughness followed an exponential law. L-Cys promotes the growth of small needle-like grains promoting a preferential growth direction perpendicular to the (220) phase, at low L-Cys concentration those structures tend to form aggregates toward the direction normal to the long side of them. The rise of brightener concentration favors the co-deposition of copper sulfides in grain borders, limiting the growth and preventing the aggregation. About the mechanism of action, the amino acid is prone to arrange itself planar to the surface, by interacting both with the thiol and the carboxylic group. The suppressor role of competing with the brightener adsorption and copper complexation is held by the supramolecular arrangement dominated by coulombic interactions within the formulation, composed by the protonated L-Cys which coordinates a double layer formed by sulphate and copper ions alternating.

CRediT authorship contribution statement

Fabio Biffoli: Writing – review & editing, Writing – original draft, Software, Investigation, Formal analysis, Conceptualization. **Pierantonio Corsi:** Visualization, Investigation, Formal analysis. **Mariano Riccardi:** Software, Investigation. **Carla Bazzicalupi:** Writing – review & editing, Writing – original draft, Supervision, Conceptualization. **Marco Bonechi:** Writing – review & editing, Writing – original draft, Validation, Supervision. **Claudio Fontanesi:** Writing – review & editing, Supervision. **Walter Giurlani:** Writing – review & editing, Writing – original draft, Supervision, Investigation, Formal analysis. **Marco Pagliai:** Writing – review & editing, Writing – original draft, Validation, Supervision, Software, Conceptualization. **Massimo Innocenti:** Writing – review & editing, Writing – original draft, Supervision, Resources, Project administration, Funding acquisition, Conceptualization.

Declaration of competing interest

The authors declare that they have no known competing financial interests or personal relationships that could have appeared to influence the work reported in this paper.

Acknowledgments

The authors thanks Regione Toscana PR FESR 2021/2027, Azione 1.1.4.1, Bando 1 “Progetti strategici di ricerca e sviluppo” which made possible the project: “Sviluppo e ottimizzazione di nuovi processi, prodotti e prototipi per il prolungamento del ciclo di vita di articoli di rubinetteria, accessori moda e gioielli” (FREEGALVAN) CUP-ST 27716.29122023.042000059. The authors acknowledge the National Recovery and

Resilience Plan (NRRP), Mission 4 Component 2 Investment 1.3 - Call for tender No. 341 of March 15, 2022 of Italian Ministry of University and Research (MUR) funded by the European Union - NextGenerationEU - Project code PE_00000004, CUP B83C22004890007, Project title “3A-ITALY - Made-in-Italy circolare e sostenibile”. The authors also acknowledge also for the support offered by Fondazione CR Firenze,

Fondazione per la Ricerca e l'Innovazione dell'Università degli Studi di Firenze and Confindustria Firenze within the FABER4 project.

Supplementary materials

Supplementary material associated with this article can be found, in the online version, at doi:10.1016/j.electacta.2025.146243.

Data availability

Data will be made available on request.

References

[1] Z. Zhao, Z. Liu, L. Chen, Q. Sun, H. Liu, Y. Sun, FEA study on the TSV copper filling influenced by the additives and electroplating process, Microelectron. Eng. 275 (2023) 111981, https://doi.org/10.1016/j.mee.2023.111981.

[2] J. Yu, J. Yang, Preparation and application method of CNTs dispersion solution for direct electroplating on circuit board holes, J. Phys. Conf. Ser. 2789 (2024) 012009, https://doi.org/10.1088/1742-6596/2789/1/012009.

[3] Z. Sun, G. He, Z. Zhao, X. He, H. Zhao, Research progress of electroplated micropore for interconnection technology, J. Phys. Conf. Ser. 2430 (2023) 012011, https://doi.org/10.1088/1742-6596/2430/1/012011.

[4] W. Chen, S. Wang, Z. Liu, C. Wei, Y. Peng, Development of bidirectional pulsed power supply and its effect on copper plating effect of printed circuit board via-filling, Electronics 12 (2023) 631, https://doi.org/10.3390/electronics12030631.

[5] W. Giurlani, G. Zangari, F. Gambinossi, M. Passaponti, E. Salvietti, F. Di Benedetto, S. Caporali, M. Innocenti, Electroplating for decorative applications: recent trends in research and development, Coatings 8 (2018) 1–25, https://doi.org/10.3390/coatings8080260.

[6] W. Giurlani, F. Biffoli, L. Fei, F. Pizzetti, M. Bonechi, C. Fontanesi, M. Innocenti, Analytic procedure for the evaluation of copper intermetallic diffusion in electroplated gold coatings with energy dispersive X-ray microanalysis, Anal. Chim. Acta 1269 (2023) 341428, https://doi.org/10.1016/j.aca.2023.341428.

[7] F. Biffoli, W. Giurlani, M. Vorobyova, I. Maccioni, C. Giovani, M. Salvi, E. Cianfanelli, M. Pagliai, M. Innocenti, Tailoring barrier layers design for haute couture through X-ray microanalysis: insights and guidelines, Heliyon 10 (2024) e32147, https://doi.org/10.1016/j.heliyon.2024.e32147.

[8] E. Mariani, W. Giurlani, M. Bonechi, V. Dell'Aquila, M. Innocenti, A systematic study of pulse and pulse reverse plating on acid copper bath for decorative and functional applications, Sci. Rep. 12 (2022) 18175, https://doi.org/10.1038/s41598-022-22650-x.

[9] M. Vorobyova, F. Biffoli, W. Giurlani, S.M. Martinuzzi, M. Linser, A. Caneschi, M. Innocenti, PVD for decorative applications: a review, Materials (Basel) 16 (2023) 4919, https://doi.org/10.3390/ma16144919.

[10] M. Verrucchi, A. Comparini, M. Bonechi, I. del Pace, G. Zangari, W. Giurlani, M. Innocenti, Electrochemical spectroscopic analysis of additives in copper plating baths by DRT and multivariate approach, J. Electroanal. Chem. 954 (2024) 118045, https://doi.org/10.1016/j.jelechem.2024.118045.

[11] Y.-H. Wang, D. Senthil Raja, D.-H. Tsai, Quantifying thiolated chemical additives for copper electroplating process, Anal. Chim. Acta 1307 (2024) 342608, https://doi.org/10.1016/j.aca.2024.342608.

[12] K. Bogomolov, E. Grishina, Y. Ein-Eli, Sulfonate compounds embraced from acid copper electroplating baths as innovative additives for alkaline Zn batteries, J. Mater. Chem. A 11 (2023) 24099–24113, https://doi.org/10.1039/D3TA04612E.

[13] H. Yang, Y. Wang, M. Chen, J. Liu, Y. Liu, T. Chen, J. Li, Research on electroplating bonding of flip-chip under the action of additives, IEEE Trans. Comp. Packag. Manuf. Technol. 13 (2023) 1324–1331, https://doi.org/10.1109/TCPMT.2023.3301184.

[14] B. Yuan, W. Zhou, X. Li, Y. Xie, X. Yin, X. Chen, D. Shen, L. Wang, Investigation of synthesized carbazole derivative Cz-BPDB as a high-performance leveler for copper electroplating, Surf. Coat. Technol. 463 (2023) 129526, https://doi.org/10.1016/j.surfcoat.2023.129526.

[15] W. Giurlani, G. Pappaianni, F. Biffoli, E. Mariani, M. Bonechi, L. Giliberti, M. Tufarelli, P. Franzo, E. Cianfanelli, M. Innocenti, What is the current state of sustainability in the decorative electroplating industry? A close look at new practices and advances, Sustainability 16 (2024) 5821, https://doi.org/10.3390/su16135821.

[16] L. Xiao, Q. Li, H. Zeng, L. Tian, X. Huang, J. Xie, H. Zhang, W. He, K. Liang, Q. Huang, Y. Chen, Investigation of azathioprine and its local-structure molecules as levelers for through-holes copper electroplating, Surf. Interfaces 53 (2024) 105073, https://doi.org/10.1016/j.surfin.2024.105073.

[17] Z.-Y. Wang, L. Jin, J.-Q. Yang, W.-Q. Li, D.-Y. Wu, D. Zhan, F.-Z. Yang, S.-G. Sun, A transfer-adsorption model for forward understanding the synergistic effects of additives in through-hole uniform copper thickening, J. Electroanal. Chem. 936 (2023) 117373, https://doi.org/10.1016/j.jelechem.2023.117373.

[18] C. Han, Y. Zhai, Y. Chen, J. Li, W. Cai, Z. Zhou, Y. Hong, C. Wang, G. Zhou, Alkyl-terminated PEG suppressors for copper electroplating and their hydrophilic and hydrophobic properties, Surf. Coat. Technol. 484 (2024) 130848, https://doi.org/10.1016/j.surfcoat.2024.130848.

[19] R. Mroczka, A. Słodkowska, A. Ładniak, A. Chrzanowska, Interaction of bis-(sodium-sulfopropyl)-disulfide and polyethylene glycol on the copper electrodeposited layer by time-of-flight secondary-ion mass spectrometry, Molecules 28 (2023) 433, https://doi.org/10.3390/molecules28010433.

[20] R. Mroczka, A. Słodkowska, The properties of the polyethylene glycol complex PEG (Na+)(Cu+) on the copper electrodeposited layer by time-of-flight secondary-ion mass spectrometry. The new insights, Electrochim. Acta 339 (2020) 135931, https://doi.org/10.1016/j.electacta.2020.135931.

[21] F. Biffoli, I. Cartechini, M. Riccardi, W. Giurlani, M. Bonechi, C. Bazzicalupi, C. Fontanesi, M. Pagliai, M. Innocenti, Clarifying the mechanism of actions of suppressor, brightener and sodium chloride in acid copper electrodeposition: a multidisciplinary approach for a many variable problem, J. Electroanal. Chem. 972 (2024) 118617, https://doi.org/10.1016/j.jelechem.2024.118617.

[22] T.M.T. Huynh, F. Weiss, N.T.M. Hai, W. Reckien, T. Bredow, A. Fluegel, M. Arnold, D. Mayer, H. Keller, P. Broekmann, On the role of halides and thiols in additive-assisted copper electroplating, Electrochim. Acta 89 (2013) 537–548, https://doi.org/10.1016/j.electacta.2012.10.152.

[23] M.H. Lee, M.J. Kim, J.J. Kim, Competitive adsorption between bromide ions and bis(3-sulfopropyl)-disulfide for Cu microvia filling, Electrochim. Acta 370 (2021) 137707, https://doi.org/10.1016/j.electacta.2020.137707.

[24] F. Soltermann, C. Abegglen, C. Götz, U. von Gunten, Bromide sources and loads in Swiss surface waters and their relevance for bromate formation during wastewater ozonation, Environ. Sci. Technol. 50 (2016) 9825–9834, https://doi.org/10.1021/acs.est.6b01142.

[25] Q.-Y. Wu, Y. Li, H.-Y. Hu, Y.-X. Sun, F.-Y. Zhao, Reduced effect of bromide on the genotoxicity in secondary effluent of a municipal wastewater treatment plant during chlorination, Environ. Sci. Technol. 44 (2010) 4924–4929, https://doi.org/10.1021/es100152j.

[26] S. Dong, N. Masalha, M.J. Plewa, T.H. Nguyen, Toxicity of wastewater with elevated bromide and iodide after chlorination, chloramination, or ozonation disinfection, Environ. Sci. Technol. 51 (2017) 9297–9304, https://doi.org/10.1021/acs.est.7b02345.

[27] T.M. Braun, D. Josell, J. John, T.P. Moffat, Editors' choice—simulation of copper electrodeposition in through-hole vias, J. Electrochem. Soc. 167 (2020) 013510, https://doi.org/10.1149/2.0102001JES.

[28] Y. Zhang, M. An, P. Yang, J. Zhang, Recent advances in electroplating of through-hole copper interconnection, Electrocatalysis 12 (2021) 619–627, https://doi.org/10.1007/s12678-021-00687-2.

[29] V.H. Waite, Electrodeposition of metals, US2112818A, 1934.

[30] J.A. Henricks, Method and electrolyte for the electrodeposition of metals, US2424887A, 1941.

[31] M.L. Freed, O.A. Stocker, Production of bright metallic deposits, US2409120, 1946.

[32] L. Guo, S. Li, Z. He, Y. Fu, F. Qiu, R. Liu, G. Yang, Electroplated copper additives for advanced packaging: a review, ACS Omega 9 (2024) 20637–20647, https://doi.org/10.1021/acsomega.4c01707.

[33] Z. Lai, S. Wang, C. Wang, Y. Hong, G. Zhou, Y. Chen, W. He, Y. Peng, D. Xiao, A comparison of typical additives for copper electroplating based on theoretical computation, Comput. Mater. Sci. 147 (2018) 95–102, https://doi.org/10.1016/j.commatsci.2017.11.049.

[34] Q. Li, J. Hu, J. Zhang, P. Yang, Y. Hu, M. An, Screening of electroplating additive for improving throwing power of copper pyrophosphate bath via molecular dynamics simulation, Chem. Phys. Lett. 757 (2020) 137848, https://doi.org/10.1016/j.cplett.2020.137848.

[35] X. Li, P. Zou, X. Chen, L. Wang, Quantum chemical calculations and molecular dynamics simulations to investigate the mechanism of interaction of six dye levelers with copper surface, J. Electroanal. Chem. 961 (2024) 118230, https://doi.org/10.1016/j.jelechem.2024.118230.

[36] R. Tao, H. Vovusha, X. Li, R. Melentiev, K. Zhu, M. Lanza, U. Schwingenschlögl, A. K. Tevtia, G. Lubineau, Characterizing ABS–copper chemistry-dependent adhesion: from the atomic to macro level, J. Mater. Res. Technol. 29 (2024) 4384–4393, https://doi.org/10.1016/j.jmrt.2024.02.158.

[37] P. Ren, R. Li, P. Yang, J. Zhang, M. An, Effect of nitrogen-containing groups on the reduction of copper ions: in situ Raman and AIMD, Surf. Interfaces 51 (2024) 104769, https://doi.org/10.1016/j.surfin.2024.104769.

[38] B. Panda, Effects of added chloride ion on electrodeposition of copper from a simulated acidic sulfate bath containing cobalt ions, ISRN Metall. 2013 (2013) 1–6, https://doi.org/10.1155/2013/930890.

[39] M. Sun, C. Zhang, R. Ya, H. He, Z. Li, W. Tian, Synergistic effects of 2-butyne-1,4-diol and chloride ions on the microstructure and residual stress of electrodeposited nickel, Materials (Basel) 16 (2023) 3598, https://doi.org/10.3390/ma16093598.

[40] B. Tadesse, M. Horne, J. Addai-Mensah, The effect of thiourea, l(−) cysteine and glycine additives on the mechanisms and kinetics of copper electrodeposition, J. Appl. Electrochem. 43 (2013) 1185–1195, https://doi.org/10.1007/s10800-013-0596-4.

[41] Y. Jiao, Z. Li, X.-Q. Liu, Z.-Q. Liu, R. Sun, Computational and experimental study of a novel L-Cysteine hydrochloride leveler for copper electroplated via fill in redistribution layers, in: Proceedings of the 24th International Conference on Electronic Packaging Technology, 2023, pp. 1–5, https://doi.org/10.1109/ICEPT59018.2023.10492348.

[42] C.A. Schneider, W.S. Rasband, K.W. Eliceiri, NIH Image to ImageJ: 25 years of image analysis, Nat. Methods 9 (2012) 671–675, https://doi.org/10.1038/nmeth.2089.

[43] H. Abrams, Grain size measurement by the intercept method, Metallography 4 (1971) 59–78, https://doi.org/10.1016/0026-0800(71)90005-X.

[44] S. Gates-Rector, T. Blanton, The powder diffraction file: a quality materials characterization database, Powder Diffr. 34 (2019) 352–360, https://doi.org/10.1017/S0885715619000812.
[45] A.M. Rashidi, M. Hayati, A. Rezaei, Prediction of the relative texture coefficient of nanocrystalline nickel coatings using artificial neural networks, Solid State Sci. 13 (2011) 1589–1593, https://doi.org/10.1016/j.solidstatesciences.2011.06.005.
[46] G. Pappaianni, W. Giurlani, M. Bonechi, N. Calisi, B. Cortigiani, C. Bazzicalupi, A. Caneschi, C. Fontanesi, M. Innocenti, Electrodeposition of MnAs-based thin-film as a possible promising candidate in spintronics applications, J. Electrochem. Soc. 171 (2024) 062502, https://doi.org/10.1149/1945-7111/ad5112.
[47] K. Momma, F. Izumi, VESTA: a three-dimensional visualization system for electronic and structural analysis, J. Appl. Crystallogr. 41 (2008) 653–658, https://doi.org/10.1107/S0021889808012016.
[48] D.A. Shirley, High-resolution X-ray photoemission spectrum of the valence bands of gold, Phys. Rev. B 5 (1972) 4709–4714, https://doi.org/10.1103/PhysRevB.5.4709.
[49] T. Susi, T. Pichler, P. Ayala, X-ray photoelectron spectroscopy of graphitic carbon nanomaterials doped with heteroatoms, Beilstein J. Nanotechnol. 6 (2015) 177–192, https://doi.org/10.3762/bjnano.6.17.
[50] C.D. Wagner, L.E. Davis, M.V. Zeller, J.A. Taylor, R.H. Raymond, L.H. Gale, Empirical atomic sensitivity factors for quantitative analysis by electron spectroscopy for chemical analysis, Surf. Interface Anal. 3 (1981) 211–225, https://doi.org/10.1002/sia.740030506.
[51] M. Ning, W. He, X. Tang, Z. Tao, X. He, L. Xiang, Y. Hu, X. Su, S. Cheng, Research on the effect of inorganic components on brightener in horizontal pulse plating solution by cyclic voltammetric stripping method, in: Proceedings of the 7th International Microsystems, Packaging, Assembly and Circuits Technology Conference, IEEE, 2012, pp. 333–336, https://doi.org/10.1109/IMPACT.2012.6420216.
[52] C.-C. Lin, C.-H. Yen, C.-C. Hu, The degradation behavior of brightener on dimensionally stable anodes during the copper electrodeposition, J. Electrochem. Soc. 166 (2019) D626–D634, https://doi.org/10.1149/2.0781913jes.
[53] M.J. Frisch, G.W. Trucks, H.B. Schlegel, G.E. Scuseria, M.A. Robb, J.R. Cheeseman, G. Scalmani, V. Barone, G.A. Petersson, H. Nakatsuji, X. Li, M. Caricato, A. V Marenich, J. Bloino, B.G. Janesko, R. Gomperts, B. Mennucci, H.P. Hratchian, J. V Ortiz, A.F. Izmaylov, J.L. Sonnenberg, D. Williams-Young, F. Ding, F. Lipparini, F. Egidi, J. Goings, B. Peng, A. Petrone, T. Henderson, D. Ranasinghe, V.G. Zakrzewski, J. Gao, N. Rega, G. Zheng, W. Liang, M. Hada, M. Ehara, K. Toyota, R. Fukuda, J. Hasegawa, M. Ishida, T. Nakajima, Y. Honda, O. Kitao, H. Nakai, T. Vreven, K. Throssell, J.A. Montgomery Jr., J.E. Peralta, F. Ogliaro, M.J. Bearpark, J.J. Heyd, E.N. Brothers, K.N. Kudin, V.N. Staroverov, T.A. Keith, R. Kobayashi, J. Normand, K. Raghavachari, A.P. Rendell, J.C. Burant, S.S. Iyengar, J. Tomasi, M. Cossi, J.M. Millam, M. Klene, C. Adamo, R. Cammi, J.W. Ochterski, R.L. Martin, K. Morokuma, O. Farkas, J.B. Foresman, D.J. Fox, Gaussian 16, (2016).
[54] A.D. Becke, Density-functional thermochemistry. III. The role of exact exchange, J. Chem. Phys. 98 (1993) 5648–5652, https://doi.org/10.1063/1.464913.
[55] S. Grimme, S. Ehrlich, L. Goerigk, Effect of the damping function in dispersion corrected density functional theory, J. Comput. Chem. 32 (2011) 1456–1465, https://doi.org/10.1002/jcc.21759.
[56] R. Ditchfield, W.J. Hehre, J.A. Pople, Self-consistent molecular-orbital methods. IX. An extended Gaussian-type basis for molecular-orbital studies of organic molecules, J. Chem. Phys. 54 (1971) 724–728, https://doi.org/10.1063/1.1674902.
[57] M.J. Frisch, J.A. Pople, J.S. Binkley, Self-consistent molecular orbital methods 25. Supplementary functions for Gaussian basis sets, J. Chem. Phys. 80 (1984) 3265–3269, https://doi.org/10.1063/1.447079.
[58] T. Clark, J. Chandrasekhar, G.W. Spitznagel, P.V.R. Schleyer, Efficient diffuse function-augmented basis sets for anion calculations. III. The 3-21+G basis set for first-row elements, Li–F, J. Comput. Chem. 4 (1983) 294–301, https://doi.org/10.1002/jcc.540040303.
[59] A.B. Nacsa, G. Czakó, Benchmark ab initio determination of the conformers, proton affinities, and gas-phase basicities of cysteine, J. Phys. Chem. A 126 (2022) 9667–9679, https://doi.org/10.1021/acs.jpca.2c07035.
[60] T. Yanai, D.P. Tew, N.C. Handy, A new hybrid exchange–correlation functional using the coulomb-attenuating method (CAM-B3LYP), Chem. Phys. Lett. 393 (2004) 51–57, https://doi.org/10.1016/j.cplett.2004.06.011.
[61] Y. Yang, M.N. Weaver, K.M. Merz, Assessment of the "6-31+G** + LANL2DZ" mixed basis set coupled with density functional theory methods and the effective core potential: prediction of heats of formation and ionization potentials for first-row-transition-metal complexes, J. Phys. Chem. A 113 (2009) 9843–9851, https://doi.org/10.1021/jp807643p.
[62] P. Rodríguez-Zamora, C.A. Cordero-Silis, J. Fabila, J.C. Luque-Ceballos, F. Buendía, A. Heredia-Barbero, I.L. Garzón, Interaction mechanisms and interface configuration of cysteine adsorbed on gold, silver, and copper nanoparticles, Langmuir 38 (2022) 5418–5427, https://doi.org/10.1021/acs.langmuir.1c03298.
[63] P.J. Hay, W.R. Wadt, Ab initio effective core potentials for molecular calculations. Potentials for the transition metal atoms Sc to Hg, J. Chem. Phys. 82 (1985) 270–283, https://doi.org/10.1063/1.448799.
[64] C. Adamo, V. Barone, Toward reliable density functional methods without adjustable parameters: the PBE0 model, J. Chem. Phys. 110 (1999) 6158–6170, https://doi.org/10.1063/1.478522.
[65] J.-D. Chai, M. Head-Gordon, Long-range corrected hybrid density functionals with damped atom–atom dispersion corrections, Phys. Chem. Chem. Phys. 10 (2008) 6615, https://doi.org/10.1039/b810189b.
[66] S. Grimme, Semiempirical hybrid density functional with perturbative second-order correlation, J. Chem. Phys. 124 (2006), https://doi.org/10.1063/1.2148954.
[67] M.J. Abraham, T. Murtola, R. Schulz, S. Páll, J.C. Smith, B. Hess, E. Lindahl, GROMACS: high performance molecular simulations through multi-level parallelism from laptops to supercomputers, SoftwareX (2015) 19–25, https://doi.org/10.1016/j.softx.2015.06.001, 1–2.
[68] W.L. Jorgensen, J. Chandrasekhar, J.D. Madura, R.W. Impey, M.L. Klein, Comparison of simple potential functions for simulating liquid water, J. Chem. Phys. 79 (1983) 926–935, https://doi.org/10.1063/1.445869.
[69] M. Pagliai, M. Macchiagodena, P. Procacci, G. Cardini, Evidence of a low–high density turning point in liquid water at ordinary temperature under pressure: a molecular dynamics study, J. Phys. Chem. Lett. 10 (2019) 6414–6418, https://doi.org/10.1021/acs.jpclett.9b02724.
[70] J. Wang, R.M. Wolf, J.W. Caldwell, P.A. Kollman, D.A. Case, Development and testing of a general amber force field, J. Comput. Chem. 25 (2004) 1157–1174, https://doi.org/10.1002/jcc.20035.
[71] K.G. Sprenger, V.W. Jaeger, J. Pfaendtner, The general AMBER force field (GAFF) can accurately predict thermodynamic and transport properties of many ionic liquids, J. Phys. Chem. B 119 (2015) 5882–5895, https://doi.org/10.1021/acs.jpcb.5b00689.
[72] P. Procacci, PrimaDORAC: a free web interface for the assignment of partial charges, chemical topology, and bonded parameters in organic or drug molecules, J. Chem. Inf. Model. 57 (2017) 1240–1245, https://doi.org/10.1021/acs.jcim.7b00145.
[73] S. Nosé, A molecular dynamics method for simulations in the canonical ensemble, Mol. Phys. 100 (2002) 191–198, https://doi.org/10.1080/00268970110089108.
[74] M. Parrinello, A. Rahman, Strain fluctuations and elastic constants, J. Chem. Phys. 76 (1982) 2662–2666, https://doi.org/10.1063/1.443248.
[75] C. Caleman, D. van der Spoel, Picosecond melting of ice by an infrared laser pulse: a simulation study, Angew. Chem. Int. Ed. 47 (2008) 1417–1420, https://doi.org/10.1002/anie.200703987.
[76] L. Guo, W. Dong, S. Zhang, Theoretical challenges in understanding the inhibition mechanism of copper corrosion in acid media in the presence of three triazole derivatives, RSC Adv. 4 (2014) 41956–41967, https://doi.org/10.1039/c4ra04931d.
[77] C.A. Huang, J.H. Chang, F.Y. Hsu, Electrocrystallization behavior of copper electrodeposited from aqueous sulfuric acid with thiourea and chloride additives, ECS Trans. 2 (2006) 329–334, https://doi.org/10.1149/1.2196021.
[78] M. Song, G. Zhou, N. Lu, J. Lee, E. Nakouzi, H. Wang, D. Li, Oriented attachment induces fivefold twins by forming and decomposing high-energy grain boundaries, Science 367 (2020) 40–45, https://doi.org/10.1126/science.aax6511, 80-.
[79] M.C. Biesinger, Advanced analysis of copper X-ray photoelectron spectra, Surf. Interface Anal. 49 (2017) 1325–1334, https://doi.org/10.1002/sia.6239.
[80] J.F. Moulder, J. Chastain, Handbook of X-ray Photoelectron Spectroscopy: A Reference Book of Standard Spectra for Identification and Interpretation of XPS Data, Physical Electronics Division, Perkin-Elmer Corporation, 1992. https://books.google.it/books?id=A_XGQgAACAAJ.
[81] B.A. Bilal, H. Tributsch, Thermo-electrochemical reduction of sulfate to sulfide using a graphite cathode, J. Appl. Electrochem. 28 (1998) 1073–1081, https://doi.org/10.1023/A:1003455219932.
[82] P. Fuentealba, P. Pérez, R. Contreras, On the condensed Fukui function, J. Chem. Phys. 113 (2000) 2544–2551, https://doi.org/10.1063/1.1305879.
[83] F. Biffoli, D. Vanossi, E. Venuti, T. Salzillo, M. Bonechi, M. Innocenti, M. Pagliai, C. Fontanesi, Charge transfer in molecular cocrystals: a plane wave vs localized-orbital view—structural information obtained from calculated Raman and IR phonons, J. Phys. Chem. C 128 (2024) 14046–14055. 10.1021/acs.jpcc.4c03470.
[84] H.R. Sudhakar, J.N. Renner, R.E. Warburton, Interfacial electric fields drive rearrangement of adsorbed cysteine and electrolyte ions on Au electrodes, J. Phys. Chem. C 128 (2024) 18063–18073, https://doi.org/10.1021/acs.jpcc.4c04216.
[85] C. Chang, Y. Chen, Y. Huang, C.-H. Lai, U.-S. Jeng, Y.-H. Lai, Nanostructured silver dendrites for photon-induced cysteine dimerization, Sci. Rep. 9 (2019) 20174, https://doi.org/10.1038/s41598-019-56517-5.
[86] M. Innocenti, L. Becucci, I. Bencistà, E. Carretti, S. Cinotti, L. Dei, F. Di Benedetto, A. Lavacchi, F. Marinelli, E. Salvietti, F. Vizza, M.L. Foresti, Electrochemical growth of Cu–Zn sulfides, J. Electroanal. Chem. 710 (2013) 17–21, https://doi.org/10.1016/j.jelechem.2013.01.024.
[87] M. Innocenti, I. Bencistà, S. Bellandi, C. Bianchini, F. Di Benedetto, A. Lavacchi, F. Vizza, M.L. Foresti, Electrochemical layer by layer growth and characterization of copper sulfur thin films on Ag(111), Electrochim. Acta 58 (2011) 599–605, https://doi.org/10.1016/j.electacta.2011.10.004.